

Chapter 1

State of the Art Methods for Estimating Backscatter Coefficients

Goutam Ghoshal, Jonathan Mamou and Michael L. Oelze

Abstract Ultrasound, which is routinely used for diagnostic imaging applications, is mainly qualitative. However, novel quantitative ultrasound techniques are being developed for diagnosing disease, classifying tissue, and assessing and monitoring the application of therapy. Ultrasound is a propagating wave that interacts with the medium as a function of the spatially-dependent mechanical properties of the medium. By analyzing the backscattered wave, various properties of the propagating media can be inferred. The backscatter coefficient, which is a fundamental material property, can be estimated from backscattered ultrasound signals and can be further parameterized for quantifying tissue properties and classifying disease. In this chapter, the history of estimating backscatter coefficients will be explored and different methods and their underlying assumptions for estimating the backscatter coefficient will be compared.

Keywords Backscatter coefficients · Spectral normalization

G. Ghoshal · M. L. Oelze (✉)
Department of Electrical Engineering, University of Illinois at Urbana-Champaign,
405 N. Mathews, Urbana, IL 61801, USA
e-mail: oelze@illinois.edu

G. Ghoshal
e-mail: ghoshal2@gmail.com

J. Mamou
F. L. Luzzi Center for Biomedical Engineering, Riverside Research, 156 William St.
9th floor, New York, NY 10038, USA
e-mail: jmamou@riversideresearch.org

1.1 Introduction

Ultrasonic scattering from biological tissue is relevant to noninvasive tissue characterization and medical diagnosis. Ultrasound is a propagating pressure wave at frequencies above the audible range in a medium that scatters and reflects acoustic energy based on the mechanical properties of different tissues. Conventional ultrasonic B-mode images are constructed from the envelope-detected, time-domain signals scattered from different tissue structures. In an ultrasonic B-mode image, the frequency dependent information resulting from the scattering media is not utilized. However, by transforming the scattered signals in the frequency domain using a Fourier transform method before B-mode processing, the frequency dependence of the scattered signals can be related to structural properties of the biological media. Often statistical modeling techniques are employed to extract sub-resolution microstructural information using ultrasound with wavelengths larger than the length scale of heterogeneity in the scattering media. To extract microstructural features, such as an effective scatterer size of the dominant microstructure, accurate estimation of the backscatter coefficient (BSC) versus frequency is necessary.

The BSC is defined as the time-averaged scattered intensity in the backward direction per unit solid angle per unit volume normalized by time-averaged incident intensity ($\text{cm}^{-1} \text{Sr}^{-1}$). Therefore, it is a fundamental quantity of a material from which microstructural properties, such as shape, size, organization, concentration and impedance mismatch between scatterers and the surrounding media, can be estimated. BSCs can be used to estimate both microstructural and acoustical properties of the tissues.

BSC-based quantitative ultrasound (QUS) has been successfully used to characterize different aspects of tissue microstructure. Numerous researchers have estimated the BSC from different organs and tissues such as ocular, liver, prostate, pancreas, spleen, renal, myocardial tissue, cardiac tissues and lymph nodes (Nicholas 1982; O'Donnell and Miller 1981; Miller et al. 1983; Lizzi et al. 1983, 1987; Fei and Shung 1985; Insana et al. 1991; Maruvada et al. 2000; Mamou et al. 2011). Topp et al. (2001) differentiated between neoplastic and healthy tissues by studying the frequency-dependent BSC from in vivo rat mammary tumors. Kabada et al. (1980) estimated BSCs to differentiate different excised canine tissues in the frequency range of 1–10 MHz. They observed a higher frequency dependence of BSC in heart (left ventricle) muscle tissue than in liver tissues. Other researchers have used BSCs to differentiate between normal dog hearts and heart tissue from dogs subjected to ischemic injury by coronary occlusion (O'Donnell et al. 1981). They hypothesized that the ultrasonic scattering was sensitive to concentration of molecular collagen and the organizational state of the structural protein. Miller et al. (1983) estimated BSC both in vitro and in vivo and observed differences between normal and ischemic dog myocardium.

Nicholas (1982) published BSCs from various human excised tissues over a frequency range of 0.7–7 MHz. The author used a power law to fit the experimental backscatter from excised human liver, spleen and brain (white matter).

The author suggested two basic scattering sites in these tissues on the order of 1 mm and 20–40 μm , respectively. D'Astous and Foster (1986) found that the BSC from tumor tissues in the female breast were virtually inseparable from those of fat at low frequencies, but began to separate at higher frequency regimes. The BSC for parenchyma of the breast was about an order of magnitude above those of fat and infiltrating ductal carcinoma.

Wear et al. (1995) published estimates of BSCs from in vivo human liver and kidney in the frequency range of 2–4 MHz. Lu et al. (1999) estimated BSC in normal human livers and human livers with diffuse diseases in vivo. Maruvada et al. (2000) estimated BSCs from bovine tissues in the frequency range of 10–30 MHz. The authors observed similar frequency dependence in BSCs between kidney and liver. Recently, Ghoshal et al. (2011) observed changes in BSCs from excised beef and rabbit livers with increasing temperature in the frequency range of 10–28 MHz. The authors observed changes in frequency dependence and amplitude of BSC with increasing temperature.

Fei and Shung (1985) used a broadband substitution technique to estimate the BSC of bovine kidney. Turnbull et al. (1989) estimated the BSC in human renal tissue and three types of renal tumors over a frequency range of 3.5–7 MHz. The authors could not differentiate between renal cell carcinoma and normal kidney tissue. Insana et al. (1991) estimated BSCs from dog kidneys using a higher frequency range of 1–15 MHz. They estimated the BSC at different angles with respect to the predominant nephron orientation and observed a frequency dependence of 1.98–2.3 depending upon the angle of incidence.

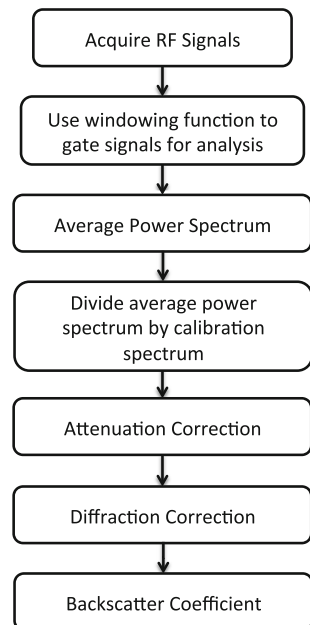
Variation in BSCs was also observed from the same in vitro tissue depending upon the histochemical fixation process. Bamber et al. (1979) demonstrated that the BSCs were different between fixed and unfixed mammalian tissue using formalin, ethyl alcohol and potassium dichromate as histochemical fixing solution. The authors suggested 4 % formalin and 5 % potassium dichromate are good for consistently preserving the ultrasonic properties within a few percent of those of the fresh tissues.

Many other researchers have utilized the BSC to classify tissues and characterize tissue states. Table 1.1 provides a compilation of some BSC results acquired by various researchers from various tissues and tissue states. Therefore, the plethora of BSC applications found in the literature suggests that the accurate and precise calculation of the BSC from ultrasonic measurements is highly important.

When correctly implemented, the estimation of the BSC is system and user independent and the BSC is only a function of the tissue properties. To estimate system- and user-independent BSCs it is necessary to account for attenuation and system effects accurately. The typical steps involved in estimating the BSC are shown in Fig. 1.1. Radio-frequency (RF) signals are acquired from a scattering media and gated using a windowing function such as Hanning or rectangular window. Next, the power spectrum of a gated signal is calculated using the Fourier transform. To improve the estimate of the BSC, the power spectra from several gated signals can be averaged providing an average power spectrum. The average power spectrum is divided by a calibration spectrum and then compensated for

Table 1.1 BSCs in soft tissues reported by various researchers

Tissue types	BSC			Reference
	$(\sigma_b = 10^{-6} \times af^n \text{ cm}^{-1} \text{ Sr}^{-1})$			
	a	n	Freq. (MHz)	
Canine liver (excised)	–	2.1	1–10	(Kabada et al. 1980)
Canine heart (excised)	–	3.3	1–10	
Dog myocardium (in vivo)	58	3.1	2–7	(Miller et al. 1983)
Dog kidney (in vitro)	1.9	2.2	1–15	(Insana et al. 1991)
Dog myocardium (in vitro)	25	3.1	1–15	(O'Donnell et al. 1981)
Bovine kidney (in vitro)	31	2.3	2–7	(Fei and Shung 1985; Shung 1993)
Bovine heart (in vitro)	0.3	3.5	10–30	(Maruvada et al. 2000)
Bovine kidney (in vitro)	4	2.5	10–30	
Bovine liver (in vitro)	5	2.4	10–30	
Human kidney (in vitro)	6.6	1.7	3.5–7	(Turnbull et al. 1989)
Human liver (excised)	270	1.2	0.7–7	(Nicholas 1982)
Human spleen (excised)	120	1.7	0.7–7	
Human brain (white matter, excised)	20	1.2	0.7–7	
Human liver (in vivo)	45	1.6	2–4	(Wear et al. 1995)
Human kidney (in vivo)	23	2.1	2–4	
Human epidermis (excised)	5	3.8		(Moran et al. 1995)
Human dermis (excised)	1.8	2.8		

Fig. 1.1 Flowchart for estimating the BSC

attenuation and diffraction effects. The resulting frequency-dependent function is known as the BSC. The main challenge to estimating the BSC is to compensate for diffraction and attenuation effects accurately.

The ability to correctly estimate the BSC has been extensively tested across different transducers and systems. In one study, ten laboratories participated in an interlaboratory study to estimate BSCs from well-calibrated tissue-mimicking phantoms using each laboratory's respective ultrasonic systems, operators and techniques (Madsen et al. 1999). The conclusion of the study was that considerable differences in BSC estimates from tissue mimicking phantoms with the same properties existed between laboratories. These differences were attributed to the different measurement techniques adopted by each group and different methods for calculating the BSC. A better agreement was observed in a subsequent interlaboratory study to compare BSCs from tissue mimicking phantoms (Wear et al. 2005). In this study, the estimated BSCs were compared with theoretical values. The theoretical BSCs were calculated using an exact solution for the scattering from the phantoms (micrometer-sized glass beads were the scatterers) and the properties of the phantoms (Faran 1951).

From the apparent lack of agreement between laboratories, more extensive studies of BSC estimation were conducted to determine the sources of error observed between different groups when estimating the BSC. In one of the subsequent studies, BSCs from tissue-mimicking phantoms, where glass beads were used as scatterers, were conducted between two laboratories (Anderson et al. 2010). The main aim was to investigate the interlaboratory comparison of the theoretical model (Faran 1951) to predict BSCs in the frequency range 1–12 MHz from glass spheres embedded in a uniform agar-based background. Overall, the results of the study demonstrated good agreement between the two laboratories (Anderson et al. 2010). Further interlaboratory comparison of BSCs from tissue-mimicking phantoms with glass beads as scatterers were conducted using four different clinical array-based imaging systems (Nam et al. 2012a, b) and again good agreement was observed.

The first interlaboratory studies demonstrated that if attenuation and diffraction effects are not accounted for accurately, the estimate of the BSC can be biased. However, later studies demonstrated that careful measurement techniques along with careful BSC calculation could provide reasonable agreement between groups suggesting that the BSC can be system and user independent. Various researchers have developed analytical and numerical methods to accurately compensate for attenuation and diffraction effects and to estimate the BSC. In this chapter, the different techniques to estimate the BSC will be examined along with the performance associated with each technique.

1.2 Methods to Estimate System Independent BSCs

1.2.1 Estimating the BSC Using Single-Element Sources

Sigelmann and Reid (1973) developed the method of estimating backscatter power from a volume of randomly distributed scatterers using a single-element planar transducer. The authors used a substitution method where the backscattered signal from a sample and planar rigid reflector are compared to estimate the volumetric backscattering cross-section. A few years later, Bamber et al. (1979) used a cylindrical tissue sample positioned with its long axis normal to the sound propagation path and recorded the backscattered signal at different angles using a planar transducer that acted both as a source and receiver. The expression for estimating the backscatter cross-section from the cylindrical tissue sample is given by (Sigelmann and Reid 1973; Bamber et al. 1979)

$$\sigma_b(\omega) = \frac{4\alpha\xi}{\Omega e^{-4\alpha r} [e^{\alpha c\tau} - e^{-\alpha c\tau}]} \frac{W_S}{W_R} \quad (1.1)$$

where α is the frequency-dependent attenuation coefficient, r is the radius of the tissue cylinder, c is the speed of sound in the tissue, τ is the duration of the time gate, Ω is the solid angle subtended by the transducer face at the center of the specimen, W_S and W_R are the measured power scattered from the tissue and the total power returned by a plane reflector and ξ is the reflection coefficient of the plane reflector.

In a later study, Nicholas et al. (1982) used the substitution method to derive the BSC given by

$$\sigma_b(\omega) = \frac{W_r}{W_i} \frac{2\eta R^2}{\beta^2 A} \left[\frac{\lambda_0}{\lambda} \right]^2 \frac{2\alpha}{e^{-2\alpha z_1} [1 - e^{\alpha c\tau}]} \quad (1.2)$$

where W_r is the total power received at the transducer face due to scattering, W_i is the total power received from a planar reflector, η is the intensity reflection coefficient for the reference interface, β is the intensity transmission coefficient for the water/tissue interface, τ is the gate duration, c is the sound speed in the tissue, R is the distance from the transducer face to the gated volume, and z_1 is the distance from the surface of the tissue to the beginning of the gated region.

D'Astous and Foster (1986) used a plane wave approximation at the focus to develop the method of computing BSCs for focused transducers. According to their calculation, the BSC may be written as

$$\sigma_b(\omega) = \frac{R_q}{2\pi(1 - \cos \theta_T)z} \frac{|S'(\omega)|^2}{|S'_0(\omega)|^2} \quad (1.3)$$

where R_q is the intensity reflectance of the water quartz interface, θ_T is the half angle of the transducer subtended at its focus, $S'(\omega)$ is the energy spectrum of the

gated, attenuation corrected signal, $S'_0(\omega)$ is the Fourier transform of the reference echo signal measured using a planar surface, and Δz is the axial length of the range gated volume.

Ueda and Ozawa (1985), derived the reference power spectrum using the boundary integral wave equation under the first order Born approximation. An approximate closed form solution for estimating the BSC assuming a Gaussian profile for the transducer radiation pattern was proposed and developed by the authors and is given by

$$\sigma_b^G(\omega) = 1.9964 \frac{(G_p/2)^2}{1 + (G_p/2)A_0\Delta z} \frac{\gamma^2 R_1^2}{A_0\Delta z} |S(\omega)|^2 \quad (1.4)$$

where ω is the frequency, A_0 is the aperture area of the transducer, Δz is the axial length of the range gated volume, R_1 is the on-axis distance between the transducer and the proximal surface of the gated volume, γ is the pressure reflection coefficient of the planar reflector, $G_p = kr^2/2R_1$ is the pressure focusing gain of the transducer (Chen et al. 1993, 1994), and a is the radius of the transducer. The power spectrum is defined by

$$|S(\omega)|^2 = \frac{\langle |S_m(\omega)|^2 \rangle}{|S_0(\omega)|^2} e^{-4(\alpha_m - \alpha_0)(R_1 + \Delta z/2)} \quad (1.5)$$

where $S_m(\omega)$ is the Fourier transform of the sample echo signal, $S_0(\omega)$ is the Fourier transform of the reference echo signal measured using a planar surface, and $\langle |S_m(\omega)|^2 \rangle$ is the average of the power spectrum of several adjacent, gated scan lines $s_m(t)$. The attenuation coefficients for the sample and the reference media are denoted by α_m and α_0 , respectively. The authors also derived the BSC for a circular piston transducer given by

$$\sigma_b(\omega) = \left(\frac{L(ka, kR_1)}{0.919} \right) 1.9964 \frac{(G_p/2)^2}{1 + (G_p/2)A_0\Delta z} \frac{\gamma^2 R_1^2}{A_0\Delta z} |S(\omega)|^2 \quad (1.6)$$

where $L(ka, kR_1)$ is a frequency-dependent correction factor, which can be calculated numerically for respective transducer characteristics (Ueda and Ozawa 1985).

Insana and co-workers (Insana et al. 1990; Insana and Hall 1990) used a volumetric integral wave equation derived under the first order Born approximation to estimate the power spectrum of both weakly scattering random media and the planar reflector. The BSC can be estimated using

$$\sigma_b(\omega) = 0.3625 \frac{\gamma^2 R_1^2}{A_0\Delta z} |S(\omega)|^2. \quad (1.7)$$

Equation (1.7) was derived assuming a Hanning window to gate the RF data. Lavarello et al. (2011) noted an inconsistency in the derivation given by Insana et al. (1990) by a factor of 16. In particular, the source function corresponding to a

planar reflector was defined as $\gamma(r_0) = \gamma' h(z_0 - z_c)$ (Insana et al. 1990, Eq. (32)) with $h(z_0 - z_c)$ a step function located at the center of the gate and γ' defined to be the planar reflection coefficient by the authors. However, if $\kappa' = \kappa_0(1 + \delta\kappa)$ and $\rho' = \rho'(1 + \delta\rho)$ and under the weak scattering assumption (i.e., $\delta\kappa, \delta\rho \ll 1$) used by the authors (Insana et al. 1990), then $\gamma' = 4\gamma$. Therefore, γ' is equal to four times the pressure reflection coefficient of the planar reflector and not to γ as stated in Insana et al (1990). As a result, the expression in Eq. (1.7) is off by a factor of 16. Therefore, Eq. (1.7) should be corrected by multiplying it by 16 (Lavarello et al. 2011).

Chen et al. determined the reference power spectrum using the mirror image method assuming a perfectly reflecting plate and derived the BSC using (Chen et al. 1994, 1997)

$$\sigma_b(\omega) = 2.17 \frac{\gamma^2 R_1^2}{A_0 \Delta z} \{ |e^{-jG_p} [J_0(G_p) + jJ_1(G_p)] - 1| \} |S(\omega)|^2 \quad (1.8)$$

where $J_m(\cdot)$ is the m th order Bessel function and $|S(\omega)|^2$ is given in Eq. (1.5).

These different formulations for calculating the BSC were constructed for single-element transducers. The variations in these different formulations can explain some of the variations observed in BSC estimates in interlaboratory comparisons of BSCs from tissue-mimicking phantoms. Additional methods for calculating BSCs from ultrasonic arrays required different normalization procedures.

1.2.2 Estimating the BSC Using Arrays

Insana and co-workers developed a method to estimate BSCs using array transducers by analyzing the transducer beam directivity function for linear, two-dimensional and annular-array transducers (Insana et al. 1994). The BSC is given by

$$\sigma_b(\omega) = \frac{2}{3L} \left(\frac{\lambda R}{A} \right)^2 \frac{W(f)}{B_H(0,0)} \quad (1.9)$$

where L is the range gate length, R is the focal length, A is the active area of the transducer, W is the normalized power density spectrum and B_H is the autocorrelation function for beam directivity. The authors provided the analytical expressions for beam directivity functions and BSC for linear, two-dimensional and annular-array transducers.

Yao et al. (1990) derived the BSC from a sample by comparing the echo data acquired from the sample with the data from a well-characterized reference sample whose BSCs and attenuation coefficients were known, i.e., the reference phantom technique. The BSC using the reference phantom technique is given by

Table 1.2 Equations for calculating the BSC developed by different authors

References	BSC ($\sigma_b(\omega)$)	Remarks
(Sigelmann and Reid 1973; Bamber et al. 1979)	$\frac{4z\xi}{\Omega e^{-4zr} [e^{2z\xi} - e^{-2z\xi}]}$	Single-element transducer
(Nicholas 1982)	$\frac{W_i}{W_o} \frac{2\eta R^2}{\beta^2 A} \left[\frac{\lambda_0}{L}\right]^2 \frac{2\pi}{e^{-2z\xi_1} [1 - e^{2z\xi}]}$	Substitution technique
(D'Astous and Foster 1986)	$\frac{R_q}{2\pi(1 - \cos \theta_T)z} \frac{ S'(\omega) ^2}{ S'_0(\omega) ^2}$	Single-element focused transducer
(Ueda and Ozawa 1985)	$1.9964 \frac{(G_p/2)^2}{1+(G_p/2)} \frac{\gamma^2 R_1^2}{A_0 \Delta z} S(\omega) ^2$	Single-element focused transducer, Gaussian beam
(Insana et al. 1990; Insana and Hall 1990)	$\left(\frac{L(ka, kR_1)}{0.919}\right) 1.9964 \frac{(G_p/2)^2}{1+(G_p/2)} \frac{\gamma^2 R_1^2}{A_0 \Delta z} S(\omega) ^2$	Circular focused transducer
(Chen et al. 1994, 1997)	$0.3625 \frac{\gamma^2 R_1^2}{A_0 \Delta z} S(\omega) ^2$	Single-element focused circular piston transducer
(Insana et al. 1994)	$2.17 \frac{\gamma^2 R_1^2}{A_0 \Delta z} S(\omega) ^2$ $\times \{ e^{-jG_p} [J_0(G_p) + jJ_1(G_p)] - 1 \}$	Single-element focused piston transducer
(Yao et al. 1990)	$\frac{2}{3L} \left(\frac{\lambda R}{A}\right)^2 \frac{W(f)}{B_H(0,0)}$ $\sigma_b^R(\omega) e^{-4z(z_R(\omega) - z_S(\omega))} \frac{ S_S(\omega) ^2}{ S_R(\omega) ^2}$	Array transducer For any source/receiver characteristics

$$\sigma_b(\omega) = \sigma_b^R(\omega) e^{-4z(z_R(\omega) - z_S(\omega))} \frac{|S_S(\omega)|^2}{|S_R(\omega)|^2} \quad (1.10)$$

where z is the depth, $\sigma_b^S(\omega)$ and $\alpha_S(\omega)$ are the backscatter and attenuation coefficients of the sample, respectively. Similarly, $\sigma_b^R(\omega)$ and $\alpha_R(\omega)$ are the backscatter and attenuation coefficients of the reference sample, respectively. The frequency domain signal from the sample and the reference sample are denoted by $S_S(\omega)$ and $S_R(\omega)$, respectively. This technique is applicable for any transducer geometry such as single-element focused/unfocused and array systems. The method assumes that the speed of sound is approximately similar both in the sample and in the reference sample.

The various methods to estimate BSCs from backscatter measurements are listed in Table 1.2. This table provides a list of the different diffraction related corrections associated with the BSC estimation.

1.2.3 Attenuation Correction

Attenuation correction is one of the major steps to estimate BSCs accurately as shown in Fig. 1.1. Typically, the frequency-dependent attenuation modifies the shape of the power spectrum which will lead to poor estimation of the BSC. Using Eq. (1.5), the normalized power spectrum is written as

$$|S(f)|^2 = \frac{|S_m(f)|^2}{|S_0(f)|^2} A(f) \quad (1.11)$$

where $A(f)$ is the frequency-dependent attenuation correction function. Extensive research has been conducted to develop attenuation correction functions. Point attenuation correction can be used for short-gated segments and low attenuation coefficients given by Oelze and O'Brien (2002)

$$A_{PC}(f) = e^{4\alpha_T(f)z_T + 2\alpha(f)L} \quad (1.12)$$

where z_T is the distance between the source and the gated region, L is the length of the gated region, and $\alpha_T(f)$, $\alpha(f)$ are the frequency-dependent attenuation coefficients in Np/cm for the intervening medium and over the gated region, respectively. Specifically, the first term accounts for the round-trip frequency-dependent attenuation losses between the gated region and the source, and the second term account for the attenuation within the gated region. The attenuation over the gated region is assumed to be constant. The point correction term also works well when using a Hanning or Hamming window to gate the RF signal.

O'Donnell and Miller (1981) used similar approximations of small gate length and low attenuation ($\alpha L > 1$) to derive an attenuation correction function given by

$$A_{OM}(f) = e^{4\alpha_T(f)z_T} \left[\frac{4\alpha(f)L}{1 - e^{-4\alpha(f)L}} \right]. \quad (1.13)$$

The above attenuation correction function is derived using a rectangular gating function. The authors chose a short gate length such that the beam function was approximately the same over the length of the gate for each frequency analyzed. The term in the square bracket accounts for frequency-dependent attenuation losses over the gated region.

Oelze and O'Brien (2002) derived another attenuation correction function by averaging the power spectra after integrating an attenuation function over the entire gate. The Oelze and O'Brien attenuation correction function is given by

$$A_{OO}(f) = e^{4\alpha_T(f)z_T} \left[\frac{2\alpha(f)L}{1 - e^{-2\alpha(f)L}} \right]^2. \quad (1.14)$$

The authors (Oelze and O'Brien 2002) demonstrated better performance than the O'Donnell and Miller (1981) model for $\alpha L < 1$ to estimate the normalized backscatter power spectrum. The authors also derived the attenuation correction function for a Hanning window given by Oelze and O'Brien (2002)

$$A_{OO}^{Han}(f) = A_{OO}(f) \left[1 + \left(\frac{2\alpha(f)L}{2\pi} \right)^2 \right]^2. \quad (1.15)$$

Bigelow and O'Brien (2004) derived attenuation correction functions by coupling the windowing function, beam pattern and attenuation coefficients. The authors

used a single order Gaussian function to model the transducer beam pattern in the focal region. The attenuation correction function is given by

$$A_{OB}(f) = e^{4z_T(f)z_T} \left[\int_{-L/2}^{L/2} dz g_{\text{win}}(z) e^{-4\frac{z^2}{w_z^2} + 4\alpha(f)z} \right]^{-1} \quad (1.16)$$

where g_{win} is the windowing function and w_z is the width of the Gaussian beam in the focal region.

Attenuation correction is one of the major components in estimating BSCs accurately. The frequency-dependent attenuation correction for some of the methods explained above are shown in Fig. 1.2a, b using $L = 1$ cm, $z_T = 0.5$ cm. The comparison between different methods for low ($\alpha_T = \alpha = 0.2$ dB/cm/MHz) and high ($\alpha_T = \alpha = 1.0$ dB/cm/MHz) attenuation coefficients is shown in Fig. 1.2a, b, respectively. The results clearly show that all the methods agree with each other for low attenuation values and start deviating as the attenuation coefficient in the sample increases. Specifically, the Oelze and O'Brien attenuation correction function lies in between the point attenuation and the O'Donnell and Miller attenuation correction function. Therefore, some attenuation correction

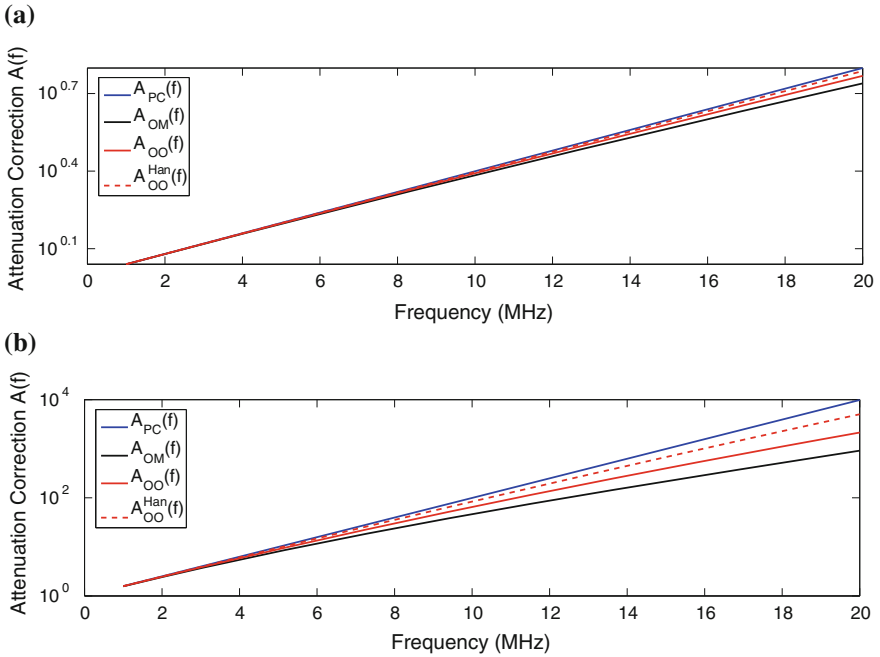


Fig. 1.2 Frequency dependent attenuation correction functions for (a) low attenuating and (b) high attenuating tissues

Table 1.3 Attenuation correction functions

References	Attenuation correction function ($A(f)$)	Remarks
(Oelze and O'Brien 2002)	$e^{4\alpha_T(f)z_T+2\alpha(f)L}$	Point attenuation correction
(O'Donnell and Miller 1981)	$e^{4\alpha_T(f)z_T} \left[\frac{4\alpha(f)L}{1-e^{-4\alpha(f)L}} \right]$	Small gate length and low attenuation
(Oelze and O'Brien 2002)	$A_{OO}(f) = \frac{e^{4\alpha_T(f)z_T-2\alpha(f)L}}{L} \left[\frac{2\alpha(f)L}{1-e^{-2\alpha(f)L}} \right]^2$	For small ($\alpha L < 1$) and large ($\alpha L > 1$) attenuation coefficients
	$A_{OO}(f) \left[1 + \left(\frac{2\alpha(f)L}{2\pi} \right)^2 \right]^2$	Hanning window
(Bigelow and O'Brien 2004)	$e^{4\alpha_T(f)z_T} \left[\int_{-L/2}^{L/2} dz g_{\text{win}}(z) e^{-4\frac{z^2}{w_z^2}+4\alpha(f)z} \right]^{-1}$	Coupled window function, beam pattern and attenuation coefficient

functions may over- or under-compensate while normalizing the power spectrum to estimate the BSC. A table of the different attenuation correction techniques that have been developed are provided in Table 1.3.

Researchers have also developed techniques to simultaneously estimate BSC and attenuation slopes using a least squares method (Nam et al. 2011). The authors used a power law model for BSCs and developed a three-parameter model to incorporate backscatter and attenuation coefficients. A least squares technique was employed to estimate backscatter and attenuation coefficients simultaneously. By simultaneously estimating the BSC and attenuation, there was no need to compensate for attenuation effects. The authors used a glass bead phantom to compare theoretical and experimental results.

1.3 Accuracy of Methods to Estimate BSCs

Given the availability of several methods for BSC estimation, it becomes of high importance to evaluate the feasibility of obtaining accurate and consistent BSC estimates. Some of the analytical models developed by various researchers are explained briefly in this chapter. Over the years, authors have developed models to predict BSCs accurately based on their experimental configurations. Lavarello et al. (2011) recently provided a comparison using three different techniques (Insana et al. 1990; Chen et al. 1997; Ueda and Ozawa 1985) shown in Eqs. (1.7), (1.8) and (1.4), respectively, to estimate BSCs from two well-characterized glass bead phantoms using multiple transducers with a wide range of focal properties and frequency bandwidths.

The basic difference between the three formulations for calculating BSCs are in the terms used to correct for diffraction effects. If these diffraction effect terms are isolated, then comparisons of their relative contributions can be conducted.

The frequency-dependent functions that are proportional to diffraction correction for each of the three formulations are given by

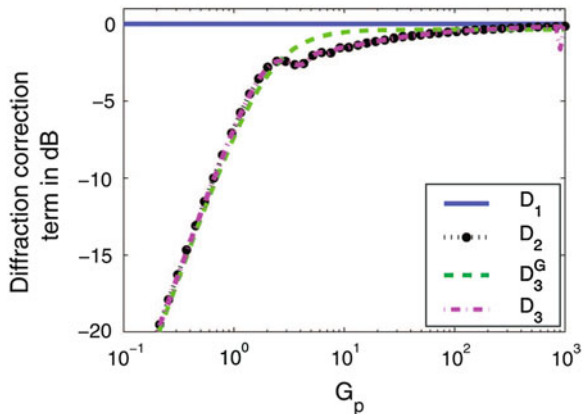
$$\begin{aligned}
 D_1(G_p) &= 1 \\
 D_2(G_p) &= |e^{-jG_p} [J_0(G_p) + jJ_1(G_p)] - 1|^2 \\
 D_3^G(G_p) &= 0.92 \frac{(G_p/2)^2}{1 + (G_p/2)^2} \\
 D_3(ka, kR_1) &= \frac{1}{0.92} D_3^G(G_p) L(ka, kR_1)
 \end{aligned} \tag{1.17}$$

where D_1, D_2, D_3^G, D_3 can be derived from Eqs. (1.7), (1.8), (1.4) and (1.6), respectively. The pressure focusing gain is given by $G_p = kr^2/2R_1$. The authors investigated the frequency dependence of three different calibration techniques as shown in Fig. 1.3. At low G_p it can be observed that all the frequency dependent calibrations terms are similar except D_1 (Insana et al. 1990) which does not have the frequency dependence.

Interestingly, all the frequency dependent calibration curves asymptotically agree with D_1 at high G_p . Specifically, the curve corresponding to D_3^G had good agreement with D_2 and D_3 for low G_p values and with D_1 for large G_p values as shown in Fig. 1.3. The curves corresponding to D_2, D_3 and D_3^G agreed with D_1 to within 1 dB for $G_p > 25$, $G_p > 25$, and $G_p > 5$, respectively. The authors demonstrated that different estimation methods introduced varying frequency-dependent effects to BSC curves, which could have noticeable effects when estimating other parameters from the BSC such as correlation length and scattering strength.

Estimates of the BSC from the two phantoms using: (1) the different transducers to cover a large frequency range, (2) a large range of G_p values, and (3) the three methods (with the Insana et al. 1990 method corrected) are plotted in Fig. 1.4. Two agar phantoms with glass bead inclusions, labeled as “41 μm phantom,” contained 47 glass spheres/ mm^3 ranging in diameter from 36 to 48 μm , and a second phantom labeled as “150–180 μm phantom,” contained 20 g/l of glass spheres (approximately 3.2 glass spheres/ mm^3) ranging in diameter from 144 to 204 μm

Fig. 1.3 Comparison of the frequency-dependent calibration terms to estimate system independent BSCs. [Figure taken from Lavarello et al. (2011)]



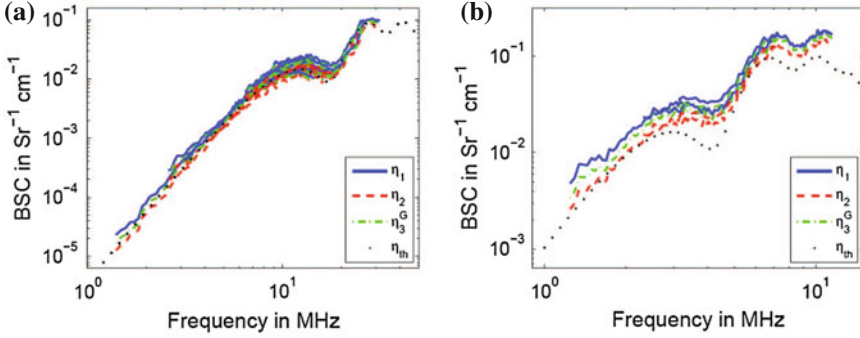


Fig. 1.4 BSC estimates from a (a) 41 μm diameter and (b) a 150–180 μm diameter glass bead phantom normalized using the three methods with the theoretical BSC for the respective phantoms. The BSCs are denoted as η_1 –(Insana et al. 1990), η_2 –(Chen et al. 1997), η_3 –(Ueda and Ozawa 1985), η_3^G –(Ueda and Ozawa 1985) assuming a Gaussian beam, and η_{th} –Farans model. [Figure taken from (Lavarello et al. 2011)]

were used for the experiments. All techniques gave similar overall BSC trends; however, there were differences in terms of the magnitude and slight differences in the frequency dependence of the BSC curves using the different methods. These differences were found to provide different estimates of scatterer size, but most estimates of scatterer size based on the BSC curves were within the range of sizes present in the phantoms as long as the ka range (acoustic wavenumber times the scatterer radius) was above 0.5.

In summary, the authors investigated several BSC normalization methods experimentally in order to isolate and determine potential differences in BSC. From experimental results, it was found that significant BSC amplitude differences may be observed depending on the normalization method used, which has a direct effect on scattering strength estimates. The differences in BSC frequency dependence introduced by all methods may result in noticeable variations in effective scatterer size estimates, especially when considering transducers with low G_p values and imaging targets with low ka products. The choice of normalization method may explain much of the variations reported in earlier inter-laboratory comparisons of BSC estimation (Madsen et al. 1999; Wear et al. 2005) and the results suggest that trying to use transducers with a larger G_p value when estimating BSCs will provide the most accurate and consistent results.

1.4 Conclusion

The ultrasonic BSC is a fundamental system-independent material quantity that can be used to characterize tissues, and monitor and assess therapies. Researchers have used BSCs to characterize different organs/tissues of the body and published

results from various mammalian tissues are available for reference for both in vitro and in vivo experimental configurations. For spectral-based QUS techniques to be successful, the BSC is one of the major parameters that needs to be estimated accurately. This is due to the fact that the BSC can be used to infer microstructural parameters such as correlation length and scattering strength. Often, correlation length can be related to cell size, as various researchers have hypothesized cells may be a dominant source of scattering in specific tissues. The scattering strength can be related to the acoustical properties of the tissue.

Due to the importance of estimating system- and user-independent BSCs accurately, numerous studies have been conducted to compensate for system effects and attenuation effects. Depending on the application, particular methods to estimate the BSC may be more appropriate based on experimental configuration and tissue types. We hypothesize that coupling attenuation and diffraction effects in an integral form (Bigelow and O'Brien 2004) can be used to estimate BSCs accurately. The method developed by Chen et al. (1997) is a robust method and used widely to estimate the BSC for focused single-element transducer systems. The reference phantom technique (Yao et al. 1990) is a very powerful technique because modeling of the diffraction pattern of the beam is not required, but the sound speed in the unknown and the reference sample need to be similar for the method to be most effective. The reference phantom technique can be used for both single-element and array transducer systems. The evidence of vast experimental and theoretical investigations conducted to estimate BSCs to infer tissue properties suggests that the BSC can be used for diagnostic and therapeutic applications.

References

- Anderson JJ, Herd MT, King MR, Haak A, Hafez ZT, Song J, Oelze ML, Madsen EL, Zagzebski JA, O'Brien WD Jr, Hall TJ (2010) Interlaboratory comparison of backscatter coefficient estimates for tissue-mimicking phantoms. *Ultrasonic Imaging* 32(1):48–64
- Bamber JC, Hill CR, King JA, Dunn F (1979) Ultrasonic propagation through fixed and unfixed tissues. *Ultrasound in Med and Biol* 5:159–165
- Bigelow TA, O'Brien WD (2004) Scatterer size estimation in pulse-echo ultrasound using focused sources: Theoretical approximation and simulation analysis. *J Acoust Soc Am* 116:578–593
- Chen X, Schwarz KQ, Parker KJ (1993) Radiation pattern of a focused transducer: A numerically convergent solution. *J Acoust Soc Am* 94:2979–2991
- Chen X, Schwarz KQ, Parker KJ (1994) Acoustic coupling from a focused transducer to a flat plate and back to the transducer. *J Acoust Soc Am* 95:3049–3054
- Chen X, Phillips D, Schwarz KQ, Mottley JG, Parker KJ (1997) The measurement of backscatter coefficient from a broadband pulse-echo system: A new formulation. *IEEE Trans Ultrason Ferroelectr Freq Control* 44:515–525
- D'Astous FT, Foster FS (1986) Frequency dependence of ultrasound attenuation and backscatter in breast tissue. *Ultrasound in Med and Biol* 12(10):795–808
- Faran JJ Jr (1951) Sound scattering by solid cylinders and spheres. *J Acoust Soc Am* 23:405–418

- Fei DY, Shung KK (1985) Ultrasonic backscatter from mammalian tissues. *J Acoust Soc Am* 78:871–876
- Ghoshal G, Luchies AC, Blue JP, Oelze ML (2011) Temperature dependent ultrasonic characterization of biological media. *J Acoust Soc Am* 130(4):2203–2211
- Insana MF, Hall TJ (1990) Parametric ultrasound imaging from backscatter coefficient measurements: Image formation and interpretation. *Ultrasonic Imag* 12:245–267
- Insana MF, Wagner RF, Brown DG, Hall TJ (1990) Describing small-scale structure in random media using pulse-echo ultrasound. *J Acoust Soc Am* 87:179–192
- Insana MF, Hall TJ, Fishback JL (1991) Identifying acoustic scattering sources in normal renal parenchyma from the anisotropy in acoustic properties. *Ultrasound in Med and Biol* 17(6):613–626
- Insana MF, Hall TJ, Cook LT (1994) Backscatter coefficient estimation using array transducers. *IEEE Trans Ultrason Ferroelectr Freq Control* 41:714–723
- Kabada MP, Bhagat PK, Wu VC (1980) Attenuation and backscattering of ultrasound in freshly excised animal tissues. *IEEE Trans Biomed Eng* 27:76–83
- Lavarello R, Ghoshal G, Oelze ML (2011) On the estimation of backscatter coefficients using single-element focused transducers. *J Acoust Soc Am* 129:2903–2911
- Lizzi FL, Greenabaum M, Feleppa EJ, Elbaum M, Coleman DJ (1983) Theoretical framework for spectrum analysis in ultrasonic tissue characterization. *J Acoust Soc Am* 73:1366–1373
- Lizzi FL, Ostromogilsky M, Feleppa EJ, Rorke MC, Yaremko MM (1987) Relationship of ultrasonic spectral parameters to features of tissue microstructure. *IEEE Trans Ultrason Ferroelectr Freq Control* 34:319–329
- Lu ZF, Zagzebski JA, Lee FT (1999) Ultrasound backscatter and attenuation in human liver with diffuse disease. *Ultrasound Med Biol* 25(7):1047–1054
- Madsen EL, Dong F, Frank GR, Gara BS, Wear KA, Wilson T, Zagzebski JA, Miller HL, Shung KK, Wang SH, Feleppa EJ, Liu T, O'Brien WD Jr, Topp KA, Sanghvi NT, Zaitzen AV, Hall TJ, Fowlkes JB, Kripfgans OD, Miller JG (1999) Interlaboratory comparison of ultrasonic backscatter, attenuation and speed measurements. *J Ultrasound Med* 18:615–631
- Mamou J, Coron A, Oelze ML, Saegusa-Beecroft E, Hata M, Lee P, Machi J, Yanagihara E, Laugier P, Feleppa EJ (2011) Three-dimensional high-frequency backscatter and envelope quantification of cancerous human lymph nodes. *Ultrasound in Med and Biol* 37:345–357
- Maruvada S, Shung KK, Wang SH (2000) High frequency backscatter and attenuation measurements of selected bovine tissue between 10 and 30 MHz. *Ultrasound Med Biol* 26(6):1043–1049
- Miller JG, Perez JE, Mottley JG, Madaras EI, Johnston PH, Blodgett ED, Thomas LJ III, Sobel BE (1983) Myocardial tissue characterization: an approach based on quantitative backscatter and attenuation. *Ultrasonic Symp Proc* 2:782–793
- Moran CM, Bush NL, Bamber JC (1995) Ultrasonic propagation properties of excised human skin. *Ultrasound in Med and Biol* 21:1177–1190
- Nam K, Zagzebski JA, Hall TJ (2011) Simultaneous backscatter and attenuation estimation using a least square method with constraints. *Ultrasound in Med and Biol* 37(12):2096–2104
- Nam K, Rosado-Mendex IM, Wirtzfeld LA, Kumar V, Madsen EL, Ghoshal G, Pawlicki AD, Oelze ML, Lavarello RJ, Bigelow TA, Zagzebski JA, O'Brien WD Jr, Hall TJ (2012a) Cross-imaging system comparison of backscatter coefficients estimates from tissue-mimicking material. *J Acoust Soc Am* 132:1319–1324
- Nam K, Rosado-Mendex IM, Wirtzfeld LA, Pawlicki AD, Kumar V, Madsen EL, Ghoshal G, Lavarello RJ, Oelze ML, Bigelow TA, Zagzebski JA, O'Brien WD Jr, Hall TJ (2012b) Ultrasonic attenuation and backscatter coefficient estimates of rodent-tumor mimicking structures: Comparison of results among clinical scanners. *Ultrasonic Imag* 33:233–250
- Nicholas D (1982) Evaluation of backscattering coefficients for excised human tissues: Results, interpretation, and associated measurements. *Ultrasound Med and Biol* 8:17–28
- O'Donnell M, Miller JG (1981) Quantitative broadband ultrasonic backscatter: An approach to nondestructive evaluation in acoustically inhomogeneous materials. *J Appl Phys* 52(2):1056–1065

- O'Donnell M, Mimbs JW, Miller JG (1981) Relationship between collagen and ultrasonic backscatter in myocardial tissue. *J Acoust Soc Am* 69(2):580–588
- Oelze ML, O'Brien WD Jr (2002) Frequency-dependent attenuation-compensation functions for ultrasonic signals backscattered from random media. *J Acoust Soc Am* 111:2308–2319
- Shung KK (1993) In vitro experimental results on ultrasonic scattering in biological tissues. In: Thieme GA (ed) Shung KK. CRC Press, *Ultrasonic Scattering in Biological Tissues*, pp 75–124
- Sigelmann RA, Reid JM (1973) Analysis and measurement of ultrasound backscattering from an ensemble of scatterers excited by sine-wave bursts. *J Acoust Soc Am* 53:1351–1355
- Topp KA, Zachary JF, O'Brien WD Jr (2001) Quantifying B-mode images of in vivo rat mammary tumors by the frequency dependence of backscatter. *J Ultrasound Med* 20:605–612
- Turnbull DH, Wilson SR, Hine AL, Foster FS (1989) Quantifying B-mode images of in vivo rat mammary tumors by the frequency dependence of backscatter. *Ultrasound in Med and Biol* 15:241–253
- Ueda M, Ozawa Y (1985) Spectral analysis of echoes for backscattering coefficient measurements. *J Acoust Soc Am* 77(38–47):
- Wear KA, Gara BS, Hall TJ (1995) Measurements of ultrasonic backscatter coefficients in human liver and kidney in vivo. *J Acoust Soc Am* 98:1852–1857
- Wear KA, Stiles TA, Frank GR, Madsen EL, Cheng F, Feleppa EJ, Hall CS, Kim BS, Lee P, O'Brien WD Jr, Oelze ML, Raju BI, Shung KK, Wilson TA, Yuan JR (2005) Interlaboratory comparison of ultrasonic backscatter coefficient measurements from 2 to 9 MHz. *J Ultrasound Med* 24:1235–1250
- Yao LX, Zagzebski JA, Madsen EL (1990) Backscatter coefficient measurements using a reference phantom to extract depth-dependent instrumentation factors. *Ultrasonic Imag* 12:58–70